IEEE Access
Multidisciplinary | Rapid Review | Open Access Journal

Received 13 September 2022, accepted 6 October 2022, date of publication 19 October 2022, date of current version 26 October 2022.

Digital Object Identifier 10.1109/ACCESS.2022.3215740

RESEARCH ARTICLE

Mitigation of Short-Term Fluctuations in Wind Power Output in a Balancing Area on the Road Toward 100% Renewable Energy

CHIYORI T. URABE[1], (Member, IEEE), TAKASHI IKEGAMI[2], (Member, IEEE), AND KAZUHIKO OGIMOTO[1], (Member, IEEE)

[1]Institute of Industrial Science, The University of Tokyo, Tokyo 153-8505, Japan
[2]Division of Advanced Mechanical Systems Engineering, Institute of Engineering, Tokyo University of Agriculture and Technology, Tokyo 184-8588, Japan

Corresponding author: Chiyori T. Urabe (chiyori@iis.u-tokyo.ac.jp)

ABSTRACT The rapid growth of the share of variable renewable energy (VRE) may make it difficult to operate power systems incorporating these sources, due to fluctuations in VRE output. In this paper, we focus on the short-term fluctuations (STFs) in wind power total outputs in several balancing areas (BAs) in Japan. We propose five methods to mitigate STFs, utilizing innate functions of wind turbines that use neither battery systems nor any other additional systems or equipment. In addition, the methods suggested do not require predictions of the wind power output. The efficiency of the method was measured based on the relationship between the mitigation of STFs and associated energy loss. Historical wind power output data from three BAs in Japan (the Hokkaido, Tohoku, and Kyushu BAs) were used to conduct numerical simulations. One of the proposed methods effectively mitigated STFs in the total wind power output. The proposed approach is applicable to solar power and will help overcome challenges on the road toward 100% renewable energy.

INDEX TERMS Energy system integration, maximum power point tracking, ramp rate limitation, short-term fluctuations, smoothing effect, wind power, 100% renewable energy.

I. INTRODUCTION

Renewable energy generation has been promoted over the last decade in an effort to reduce greenhouse gas emissions, with wind power and solar power use seeing sharp increases. The global production of wind and solar power increased from 377 TWh in 2010 to 2,105 TWh in 2019, representing an approximately six-fold increase; in Japan, the production of wind and solar power increased ten-fold from 2010 to 2019 [1], [2].

Wind and solar power are variable renewable energy (VRE) sources, where the outputs of VRE can change rapidly according to the weather conditions. An increase in VRE power generation amplifies fluctuations in VRE output, whereas smoothing mitigates fluctuations via appropriate VRE output and geographical distributions of VRE power plants. However, VRE resources tend to be localized [3]; many wind sources in Japan are located in its northern regions, and VRE output is characterized by seasonality, with wind power output increases observed in winter [4], [5], [6]. Fluctuations in wind power output can negatively impact the stability of the power system [5], [7], [8], [9], [10].

Regarding power system operation, fluctuations in VRE output are compensated for by changes in the outputs of hydroelectric and thermal power plants, batteries, and other VRE sources in the local balancing area (BA), or in other BAs through interconnections. In recent years, power markets have supplied a portion of the reserves in response to VRE fluctuations. The reserves are categorized according to timescale, as frequency containment reserves (FCRs), frequency restoration reserves (FRRs), and replacement reserves (RRs), as shown in Fig. 1.

As the world moves toward 100% renewable energy (RE100), the required reserves will increase [5], [7], [9], whereas traditional reserves will decrease as thermal power plants are retired. In Japan, the wind power capacity increased

The associate editor coordinating the review of this manuscript and approving it for publication was Mouloud Denai.

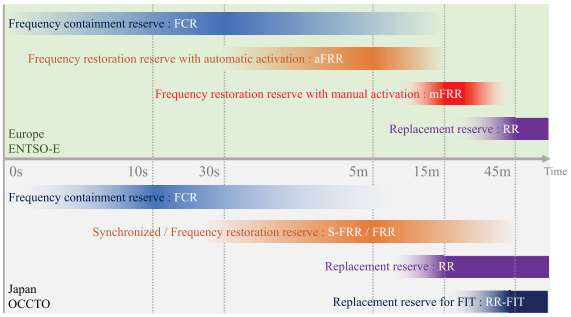

FIGURE 1. Reserves in Europe (upper) [11] and Japan (bottom) [12]. The color intensity indicates the amount of reserves provided. While synchronized frequency restoration reserves (S-FRRs) and FRRs have the same timescale, power plants providing the S-FRRs are required to always be connected to the power system. In Japan, the operation of reserves is a topic of discussion by the Organization for Cross-regional Coordination of Transmission Operators (OCCTO).

from 2,613 MW in the financial year (FY) 2012 to 4,438 MW in FY2020 [13], while the demand decreased from 912 TWh in FY2012 to 864 TWh in FY2020 [14]. Impact of fluctuations in wind power output would magnify because the share of wind power increased. Potential resources for energy reserves include VRE and battery storage. VRE resources can provide reserves by reducing power generation. Battery storage is another promising option for providing reserves for a power system with a high share of VRE; however, the installation cost is high. Thus, on the road toward RE100, other options should be considered to overcome the challenge of providing the necessary reserves.

To reduce the required reserves, we focused on mitigating short-term fluctuations (STFs), which have the same timescale with FRRs in Fig. 1, in wind power output, utilizing functions already incorporated in wind turbines: ramp rate limitation (RRL) and maximum power point tracking (MPPT) [15], [16], [17], [18], [19], [20], [21], [22], [23]. These functions are also required in IEC 61400-1, IEC 61400-3-1, and IEC TS 61400-3-2, in which design requirements for onshore (IEC 61400-1) and offshore wind turbines (IEC 61400-3-1 and IEC TS 61400-3-2) are described [24], [25], [26]. We assumed that signals of limitations of the MPPT are sent from an aggregator, while the parameter of the RRL remains fixed. We propose five methods to mitigate STFs in the total wind power output in each BA, and compare the methods in terms of efficiency, which is indicated by the reduction in the absolute values of the STFs and the energy loss associated with application of the method. There are a number of studies on mitigation of the fluctuations in wind power output of single wind power plants (WPPs) and/or small systems consisting of several WPPs, and on the contribution of such mitigation to power systems [17], [18], [22], [23], [27], [28], [29], [30], [31], [32], [33], [34], [35], [36], [37], [38], [39]. In this study, we targeted the STFs in the total output of wind power in each BA and provide a framework for mitigating STFs.

We adopted a definition of the STFs, which uses the centered moving averages (CMAs) [6], [40]. The STFs cover a

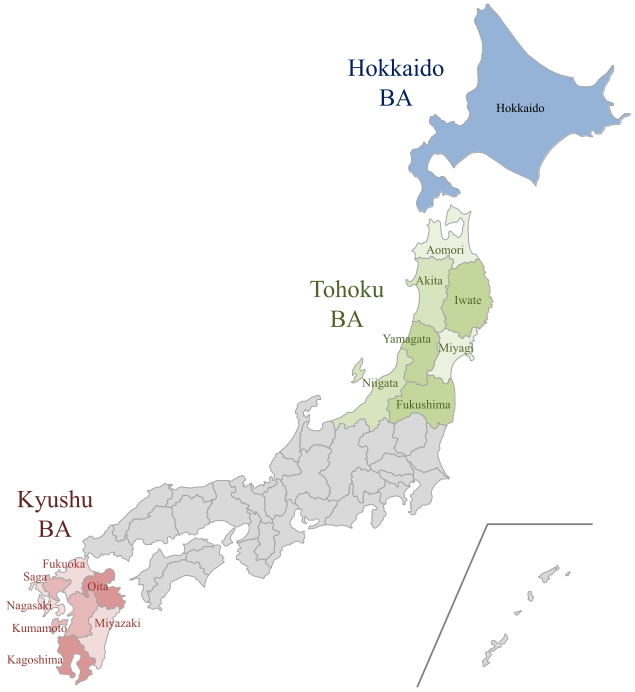

FIGURE 2. Three balancing areas (BAs): the Hokkaido, Tohoku, and Kyushu BAs.

wide timescale range and correspond to the FRRs and RRs shown in Fig. 1. We evaluated mitigation methods using historical wind power output data for three Japanese BAs for 1 year: two northern BAs (the Hokkaido and Tohoku BAs), and one southern BA, the Kyushu BA, as shown in Fig. 2. The three BAs have different characteristics. Wind power output in the northern BAs increases in winter, whereas that of the southern BA tends to be more uniform throughout the year [6].

The proposed methods were further categorized into ideal and available methods. Ideal methods use the total wind power output from each BA. The associated STFs in the total wind power output are already mitigated by the smoothing effect provided by aggregating the wind power outputs from all WPPs in the BA [41], [42], [43], [44], [45]. Therefore, the ideal methods are highly effective and involve less energy loss. However, in the real world, it is impossible to directly regulate the total output. The available methods use the wind power output from each WPP to mitigate STFs in the total wind power output from the BA. Although the efficiency of the available methods is lower than that of ideal ones (which benefit from smoothing effects), the available methods can be applied through wind farm controllers (WFCs) in individual WPPs. Therefore, mitigation of STFs using the ideal methods is done here as a reference to estimate the efficiency of the available methods.

We evaluated the methods according to efficiency, which is represented by the relationship between the mitigation of STFs in the total output of wind power and the energy loss of the method. Although the efficiency of the ideal methods was highest among all methods, through numerical simulations,

TABLE 1. Historical total wind power output data in the three balancing areas.

	Hokkaido BA	Tohoku BA	Kyushu BA
Time resolution (s)	3	10	2.5
Capacity (kW)	195,300	442,300	306,700
Number of WPPs	13	20	16
Rate of missing data* (%)	12.5	0.0	0.0

WPPs : Wind Power Plants
∗ The rate of the number of missing data is relative to the number of the entire dataset.

we found that the efficiency of one of the available methods approached that of the ideal methods. The available method is a new approach and has not been previously researched for the purpose of mitigating the STFs in the total wind power output in each BA.

The remainder of this paper is organized as follows. The historical wind power output data and the STFs in the wind power output are presented in Section II. The methods used to mitigate STFs in wind power output are described in Section III. Method evaluation is addressed in Section IV. The simulation and evaluation results for the proposed methods are presented in Section V. Finally, the conclusion and discussion are given in Section VI.

II. WIND POWER OUTPUT DATA AND SHORT-TERM FLUCTUATIONS IN OUTPUTS

To evaluate methods to mitigate STFs in the total wind power output, we used historical wind power output data obtained from three BAs (the Hokkaido, Tohoku, and Kyushu BAs of Japan), as shown in Fig. 2. The BAs have different features, as described in Sections II-A and II-C.

There are two types of data: the total output of wind power in each BA and the outputs of individual WPPs in each BA. In this paper, the total output represents the total output of wind power in each BA; individual output refers to the output of each WPP. The STFs mitigated by method application were quantified relative to the STFs in the original total output, as detailed in Section II-B.

The characteristics of the time series of the total outputs were reported in a previous study [6]. The STFs were separated from the time series of the total output using CMAs [6], [40].

A. HISTORICAL WIND POWER OUTPUT DATA

The historical time series (from 1 April 2012 to 31 March 2013) of wind power output data from the three BAs in 1 year were analyzed; the data are listed in Table 1. The time resolution was sufficiently high to separate STFs from the time series.

The wind power capacity was largest in the Tohoku BA and smallest in the Hokkaido BA. Although the Tohoku BA has the largest number of WPPs, the plants are concentrated in a narrow zone, thus weakening geographical smoothing effects [40]. Notably, each BA had some missing data, as described in Appendix A.

There are two types of output data: the total output and the individual output. Both data types have the same time resolution for each BA. When missing WPP data were identified, we did not use the other "individual data" from the same period. The total output was calculated using the individual data. Therefore, the missing data periods are the same between the total and individual datasets. In each time step, the sum of all individual outputs (kW) from a BA corresponds to the total output (kW) from the BA. The total and individual outputs are represented by p.u., unless otherwise noted. We assumed that 1 p.u. in the total and individual outputs indicates the maximum output, as it corresponds to the wind power capacity of the BA and WPP. The data and outputs before STF mitigation are referred to as the original data and outputs, respectively.

The Hokkaido and Tohoku BAs are located in the north of Japan and experience many windy days in winter. Therefore, the monthly average of the original total output increases in winter, as shown in Figs. 3 and 4. The Kyushu BA has a more uniform output during the year, as shown in Fig. 5. Because the amplitude of the STFs has a positive correlation with the monthly average output [6], the original STF amplitude tended to be large in winter for the Hokkaido and Tohoku BAs.

B. SEPARATION OF SHORT-TERM FLUCTUATIONS

The output time series are separated into very short-term fluctuations (VSTFs), STFs, and long-term fluctuations (LTFs), using two CMAs [6], [40]. The VSTFs, STFs, and LTFs have timescales of less than 1 minute, several tens of minutes, and longer, respectively. The CMAs are X- and Y-min CMAs, where X is smaller than Y. In this paper, X and Y are set to 1 and 30 minutes, respectively. The VSTFs are given by the difference between the output and X-min CMA. The STFs are given by the difference between the X-min and Y-min CMAs. The LTFs are expressed by the Y-min CMA. For convenience, the X-min and Y-min are represented by X_s and Y_s-sec in the equations.

The output at time $t = i\Delta t$ is expressed by $p(t)$, where Δt represents the time step of the output time series. In this paper, t means $i\Delta t$ unless otherwise noted. The VSTFs, STFs, and LTFs are given by the following equations, as $V(t)$, $S(t)$, and $L(t)$, respectively:

$$V(t) = p(t) - \frac{\sum_{j=-n_x}^{n_x} p(t+j\Delta t)}{2n_x+1}, \tag{1}$$

$$S(t) = \frac{\sum_{j=-n_x}^{n_x} p(t+j\Delta t)}{2n_x+1} - \frac{\sum_{j=-n_y}^{n_y} p(t+j\Delta t)}{2n_y+1}, \tag{2}$$

$$L(t) = \frac{\sum_{j=-n_y}^{n_y} p(t+j\Delta t)}{2n_y+1}, \tag{3}$$

where $n_x = X_s/2\Delta t$ and $n_y = Y_s/2\Delta t$. The sum of V, S, and L corresponds to the output p; thus, $p(t) = V(t) + S(t) + L(t)$. In this paper, the VSTF, STF, and LTF are represented by p.u.

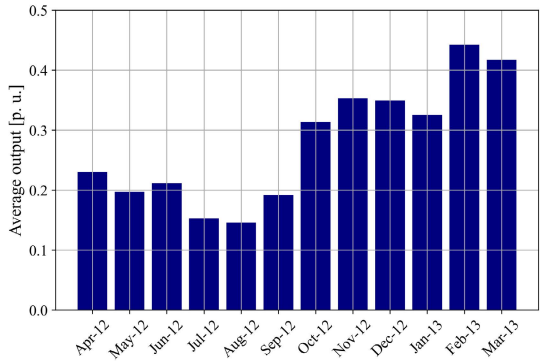

FIGURE 3. Monthly average output of the original total wind power in the Hokkaido BA.

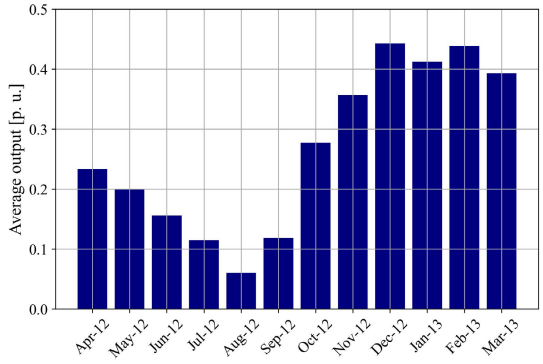

FIGURE 4. Monthly average output of the original total wind power in the Tohoku BA.

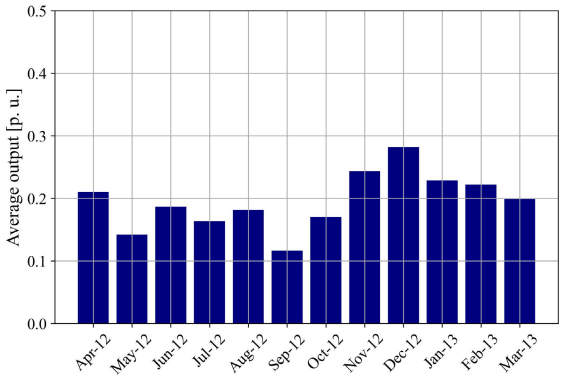

FIGURE 5. Monthly average output of the original total wind power in the Kyushu BA.

C. SHORT-TERM FLUCTUATIONS IN WIND POWER OUTPUT

The STFs in the original outputs of the three BAs were detailed in a previous study [6]. The 10th and 90th percentiles of the STFs in the original total outputs are shown in Table 2. The amplitudes of the STFs in the Hokkaido BA were the largest among the three BAs; the amplitudes of the STFs in the Tohoku and Kyushu BAs were at the same level.

The STF amplitude in the original total output in each BA tended to be small when the total capacity of wind power in the BA was large. For instance, The Hokkaido BA had the lowest total wind power capacity and a relatively large STF amplitude, as shown in Table 1.

TABLE 2. The 10th and 90th percentiles of the STFs in the original total outputs in the three BAs.

Balancing Area	Hokkaido BA	Tohoku BA	Kyushu BA
10% (p.u.)	−0.013	−0.009	−0.009
90% (p.u.)	0.013	0.010	0.009

TABLE 3. Mitigation methods: the ideal and available methods.

	Utilized functions	
Categories (used data)	RRL	MPPT
Ideal (total outputs)	T-RRL	T-MPL
Available (individual outputs)	I-RRL	I-MPL and I-AMPL

In addition, the amplitudes of the STFs increased linearly with the monthly average LTFs, and the linear function that approximates the amplitude of the STFs by the average LTFs showed a steeper gradient when the capacity of wind power in the BA was smaller [6].

The effectiveness of a particular mitigation method was evaluated based on the relationship between the reduction in the absolute values of STFs and the energy loss associated with application of the method. The reduction is expressed as the difference between the percentiles in Table 2 and those of the method-induced STF mitigation.

III. METHODS TO MITIGATE THE SHORT-TERM FLUCTUATIONS

The methods used to mitigate the STFs apply two functions of recent wind turbine designs, the RRL and MPPT, via WFCs. The WFC controls each wind turbine in the WPP according to the control parameters and signals received from an aggregator. Parameters of the RRL are fixed and set in each WFC before the implementation of the mitigation methods, while parameters of the MPPT change temporally, depending on the received signals. The RRL is able to limit the increase in output over a certain time interval, according to the control parameter. The MPPT ensures that the output remains below the upper limit, according to the control signal. Implementation of both functions involves energy loss.

Five methods, i.e., the T-RRL, T-MPL, I-RRL, I-MPL, and I-AMPL, are listed in Table 3. T and I indicate the data used, corresponding to the total and individual outputs, respectively. RRL, MPL, and AMPL indicate Ramp Rate Limitation, Maximum Power Limitation, and Advanced Maximum Power Limitation, respectively. MPL and AMPL utilize the MPPT. Thus, the methods are categorized in accordance with the data or function used.

T-RRL and T-MPL employ the total output data and cannot be implemented in the real world, because the total output (kW), given by the summation of the individual outputs (kW), cannot be controlled directly. In this paper, they are considered ideal methods. The available methods include I-RRL, I-MPL, and I-AMPL, as they use individual data. STF mitigation using the ideal methods represents the best-case scenario among methods utilizing the same function, as they involve the use of smoothing effects. As such, the ideal methods are used for reference.

T-RRL and I-RRL both utilize RRL; T-MPL, I-MPL, and I-AMPL use MPPT. A parameter of the RRL is set in

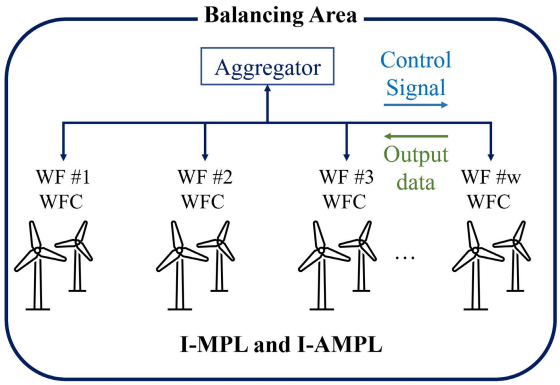

FIGURE 6. Schematic image of I-MPL and I-AMPL.

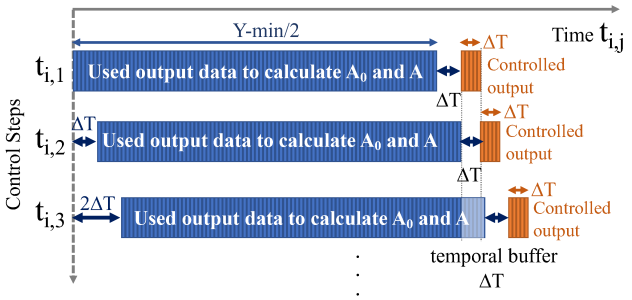

FIGURE 7. T-MPL, I-MPL, and I-AMPL limit the output over the time range $[(j+1)\Delta T + Y_s/2, (j+2)\Delta T + Y_s/2 - \Delta t]$, using past output data over the time range $[j\Delta T, j\Delta T + Y_s/2]$, as expressed in Eqs. (6)–(9) for T-MPL, Eq. (10) for I-MPL, and Eqs. (11)–(16) for I-AMPL.

each WPP and fixed during a simulation. MPPT keeps the wind power output below an upper limit. The upper limit changes according to a control signal sent from the aggregator, as shown in Fig. 6. We assumed that the WFC in each WPP appropriately controls each wind turbine according to the received control signals. T-MPL, I-MPL, and I-AMPL provide the upper limit values. Although I-MPL and I-AMPL use individual outputs, they differ in terms of the way that they share the reduction of the output when the available outputs are over the upper limit.

A. PROCEDURES OF T-RRL AND I-RRL

T-RRL can limit the increase in total output, expressed as $p(t) - \tilde{p}(t - \Delta t) \leq \Delta t/\beta$ (p.u.), where β is a parameter indicating the upper limit of the slope; the output can increase from 0 to 1 (p.u.) in β-sec. $\tilde{p}(t - \Delta t)$ represents the past total output, which is limited by T-RRL. The increment of the output is retained at a level below the upper limit $\Delta t/\beta$, as follows:

$$\tilde{p}(t) = \begin{cases} p(t), & \text{if } p(t) \leq \tilde{p}(t - \Delta t) + \Delta t/\beta, \\ \tilde{p}(t - \Delta t) + \Delta t/\beta, & \text{otherwise.} \end{cases} \tag{4}$$

When β is large, the increase in total output is limited to a small range. Therefore, the fluctuations in output are strongly mitigated as β increases, while the energy loss increases.

I-RRL limits the individual outputs, $P_k(t)(k = 1, \ldots, w)$, where w is the number of WPPs in the BA. The limitation of I-RRL is expressed by a similar equation to Eq. (4) in which p and $\tilde{p}$ of I-RRL are replaced by the individual outputs; thus, $P_k(t)$ and $\tilde{P}_k(t)$ $(k = 1, \ldots, w)$, respectively. The value of β is common to all WPPs. Therefore, the equation for I-RRL can be expressed as follows:

$$\tilde{P}_k(t) = \begin{cases} P_k(t), & \text{if } P_k(t) \leq \tilde{P}_k(t - \Delta t) + \Delta t/\beta, \\ \tilde{P}_k(t - \Delta t) + \Delta t/\beta, & \text{otherwise.} \end{cases} \tag{5}$$

B. PROCEDURES OF T-MPL AND I-MPL

T-MPL and I-MPL keep the total and individual outputs below an upper limit that changes depending on the CMA values. An aggregator sends the value of the upper limit as a control signal, as shown in Fig. 6. In the real world, because data are transferred between the aggregator and WPPs, calculations of the upper limit can induce a time lag. Therefore, in simulations of T-MPL and I-MPL, we set up a temporal buffer between the output data used to calculate the upper limit and the output data applied to the upper limit, as shown in Fig. 7.

T-MPL uses the total output and keeps it below the upper limit. Because the STFs are calculated using the Y-min CMAs, as expressed in Eq.(2), it is desirable that the upper limit be decided by the Y-min CMAs to mitigate STFs. Notably, the Y-min CMA at time t is not available at the same time t in the real world, because calculations of the Y-min CMAs at time t require output data from $t - Y_s/2$ to $t + Y_s/2$, in which the output data between t and $t + Y_s/2$ are the future data. Therefore, the Y-min CMAs are substituted by Eq. (8), which uses only the past output data in $[t - \Delta T - y/2, t - \Delta T]$ to control the output over a certain time range $[t, t + \Delta T]$. We assume that $\Delta T = 60$-sec. The total power output at $t_{i,j}$, $p(t_{i,j})$, is limited to under $A_0 + \alpha$ $(0 < \alpha < 1)$, as follows:

$$t_{i,j} = i\Delta t + j\Delta T + Y_s/2, \tag{6}$$

$$\tilde{p}(t_{i,j}) = \begin{cases} p(t_{i,j}), & \text{if } p(t_{i,j}) \leq A_0(j-1) + \alpha, \\ A_0(j-1) + \alpha, & \text{otherwise,} \end{cases} \tag{7}$$

$$A_0(j-1) = \frac{a_0(j-1) + \tilde{p}(t_{0,j-1})}{2}, \tag{8}$$

$$a_0(j-1) = \frac{2\Delta t}{Y_s} \sum_{k=1}^{\frac{Y_s}{2\Delta t}} \tilde{p}(t_{0,j-1} - k\Delta t), \tag{9}$$

where $i = 0, 1, \ldots, \Delta T/\Delta t - 1$ and $j = 1, 2, \ldots$. In the case of small α, T-MPL strongly mitigates the STFs in the total output and induces a large energy loss.

I-MPL uses the individual output P_k and is expressed by Eq. (10), which has a formula similar to that of Eq. (7). We note that $p(t_{i,j}) = \sum_{k=1}^{w} C_k P_k(t_{i,j})/c$ and $\tilde{p}(t_{i,j}) = \sum_{k=1}^{w} C_k \tilde{P}_k(t_{i,j})/c$, where the total wind power capacity and wind power capacity of the kth WPP are represented by c (kW) and C_k (kW), respectively. The individual output is

reduced by I-MPL, as follows:

$$\tilde{P}_k(t_{i,j}) = \begin{cases} P_k(t_{i,j}), & \text{if } P_k(t_{i,j}) \le A_0(j-1) + \alpha, \\ A_0(j-1) + \alpha, & \text{otherwise.} \end{cases} \tag{10}$$

The upper limit of I-MPL corresponds to $A_0 + \alpha$, as with Eq. (7). Energy loss by I-MPL increases as α decreases.

C. PROCEDURE OF I-AMPL

I-AMPL utilizes the same function as T-MPL and I-MPL, and uses the same data as I-MPL, i.e., the individual data. However, there are two differences between I-AMPL and I-MPL. The first difference pertains to calculation of the required reduction of the total output, $d(j-1)$ $(j = 1, 2, \dots)$ as follows:

$$d(j-1) = \tilde{p}(t_{0,j-1}) - A(j-1), \tag{11}$$

$$A(j-1) = \frac{a_0(j-1) + a_1(j-1)}{2}, \tag{12}$$

$$a_1(j-1) = \frac{\Delta t}{\Delta T} \sum_{k=0}^{\frac{\Delta T}{\Delta t}-1} \tilde{p}(t_{0,j-1} - k\Delta t), \tag{13}$$

where $t_{0,j} = j\Delta T + Y_s/2$ $(j = 1, 2, \dots)$, $a_0(j-1)$ is expressed in Eq. (9). The total output $\tilde{p}(t_{i,j})$ is calculated using the individual outputs; thus, $\tilde{p}(t_{i,j}) = \sum_{k=1}^{w} C_k \tilde{P}_k(t_{i,j})/c$. Here, $A(j-1)$ is similar to $A_0(j-1)$ in Eq. (8). The difference between $A(j-1)$ and $A_0(j-1)$ is $a_1(j-1)$, which is the X-min average adopted to remove the influence of single events in the total output.

The second difference concerns the way in which the required reduction $d(j-1)$ is shared among the individual WPPs. The reduction of the kth WPP, $D_k(j-1)$ (kW), is calculated from the total capacity, c (kW), and the capacity of the kth WPP, C_k (kW), as follows:

$$D_k(j-1) = cd(j-1)r_k(j-1), \tag{14}$$

$$r_k(j-1) = \frac{C_k \tilde{P}_k(t_{0,j-1})}{c\tilde{p}(t_{0,j-1})}, \tag{15}$$

where $r_k(j-1)$ indicates the proportion of the individual output of the kth WPP, $\tilde{P}(t_{0,j-1})$, relative to the total output, $\tilde{p}(t_{0,j-1})$, at time $t_{0,j-1}$.

I-AMPL reduces the individual output, as (16), shown at the bottom of the page, where $i = 0, 1, \dots, \Delta T/\Delta t - 1$. The temporal buffer between the output data used to calculate the upper limit and output data applied in the limitation is the same as those of T-MPL and I-MPL, as shown in Fig. 7. Note that $D_k(j-1)$ (kW) is converted to $D_k(j-1)/C_k$ (p.u.) in Eq. (16).

IV. EVALUATION OF THE METHODS BASED ON MITIGATION OF SHORT-TERM FLUCTUATIONS AND ENERGY LOSS

Strong mitigation of STFs tends to involve a large energy loss. On the other hand, a large energy loss does not always result from strong mitigation. The balance between the mitigation of STFs and energy loss is important for determining the most appropriate method.

A. MEASURING MITIGATION OF THE SHORT-TERM FLUCTUATIONS

To evaluate the mitigation methods, we used the 10th and 90th percentiles of the STFs in the total outputs. Percentiles are simple indicators. Those percentiles were chosen to allow general assessment of STF mitigation. The 10th and 90th percentiles are more stable than the minimum, maximum, and the 1st and 99th percentiles in all seasons [6]. For instance, the minimum, maximum, and 1st and 99th percentile values can fluctuate violently under a single extreme event and depend on chance. Therefore, these values are not suitable to measure mitigation.

The 10th and 90th STF percentiles in the original outputs in Table 2 are adopted as the baseline and compared with those for the mitigated total outputs; the difference reflects the extent of STF mitigation.

B. CALCULATION OF ENERGY LOSS

The energy loss, ΔE, is given by the difference between the original total output, $p(i\Delta t)$, and mitigated total output for a given method, $\tilde{p}(i\Delta t)$, as follows:

$$\Delta E = \frac{\sum_{i=1}^{N} p(i\Delta t) - \sum_{i=1}^{N} \tilde{p}(i\Delta t)}{\sum_{i=1}^{N} p(i\Delta t)}. \tag{17}$$

Note that $p(i\Delta t) \ge \tilde{p}(i\Delta t)$, and $\sum_{i=1}^{N} p(i\Delta t) \ge \sum_{i=1}^{N} \tilde{p}(i\Delta t)$, where N is the total number of the data. ΔE is in the range of $0 \le \Delta E \le 1$ and is represented as a percentage.

V. MITIGATION OF THE SHORT-TERM FLUCTUATIONS BY THE PROPOSED METHODS

There are five methods as shown in Table 3. Mitigations of the STFs by each method are shown in Figs. 8-12. The 10th and 90th STF percentiles relative to the total output change with parameters α and β. The percentiles in the original outputs are represented by gray dashed lines in the figures. There is a trade-off between mitigation of the STFs and energy loss. When the absolute values of percentiles are reduced by a mitigation method, the energy loss which is involved by the method increases. The parameters α and β also change the mitigation of the STFs. When α is small, the absolute values of percentiles decrease, and the energy loss increases. When

$$\tilde{P}_k(t_{i,j}) = \begin{cases} P_k(t_{i,j}), & \text{if } \alpha - D_k(j-1)/C_k \ge 0, \\ P_k(t_{i,j}) + \alpha - D_k(j-1)/C_k, & \text{otherwise,} \end{cases} \tag{16}$$

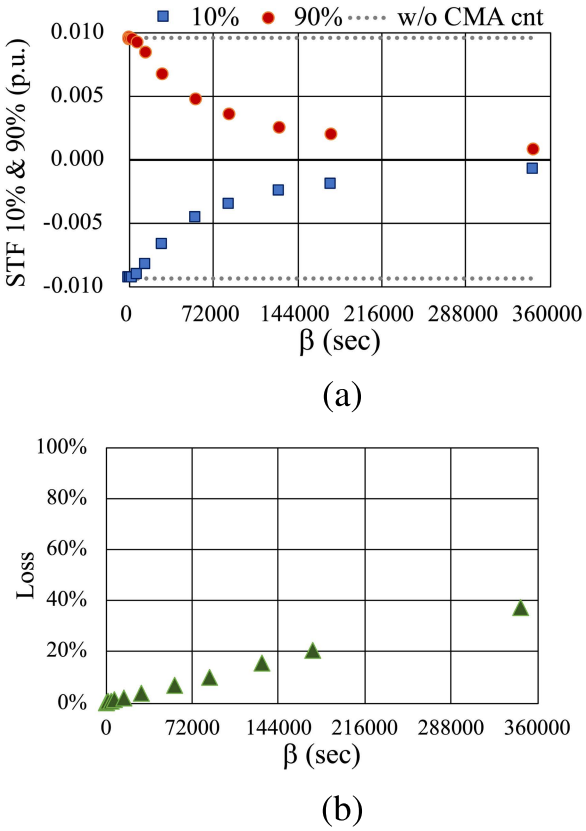

FIGURE 8. Mitigation of the STFs by T-RRL in the Tohoku BA. (a) The absolute values of the 10th and 90th percentiles of the STFs decrease with β. (b) Energy loss increases with β.

β is large, which means increment of output is retained below a small value, the absolute values of percentiles reduce, and the energy loss increases.

The methods reduce wind power output; they reduce not only the 90th percentiles, but also the 10th percentiles. The STFs are expressed as differences from the Y-min CMAs, calculated using Eq. (2). The average of the STFs is around zero. Therefore, the Y-min CMAs are around the 50th percentiles, and the STF $S = 0$. The 10th and 90th percentiles are about the same distance from $S = 0$. Consequently, the 10th and 90th percentiles change symmetrically with respect to $S = 0$.

Mitigation of STFs by T-RRL in the Tohoku BA is shown in Fig. 8. T-RRL is an ideal method for mitigating STFs. The absolute values of the 10th and 90th percentiles decreased almost linearly from $\beta = 0$ to $\beta = 72{,}000$-sec, as shown in Fig. 8 (a). While the decrease in percentiles slowed when β was larger than 72,000, the energy loss increased linearly with β, as shown in Fig. 8 (b). The relationship between the percentiles and energy loss indicates that T-RRL is efficient when $\beta < 72{,}000$.

Mitigation of STFs by T-MPL in the Tohoku BA is shown in Fig. 9. T-MPL is an ideal method to mitigate STFs. T-MPL keeps the total output below the upper limit defined in Eqs. (7)–(9). It should be mentioned that T-MPL uses output data up to 1 minute before to calculate the upper limit of output, while T-RRL can use the most recent output data. The

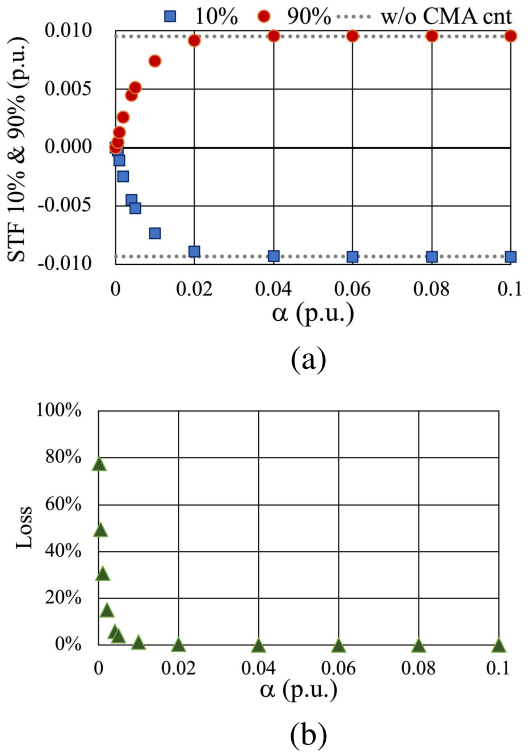

FIGURE 9. Mitigation of STFs by T-MPL in the Tohoku BA. (a) The absolute values of the 10th and 90th percentiles of the STFs decreased with α. (b) Energy loss increased as α decreased.

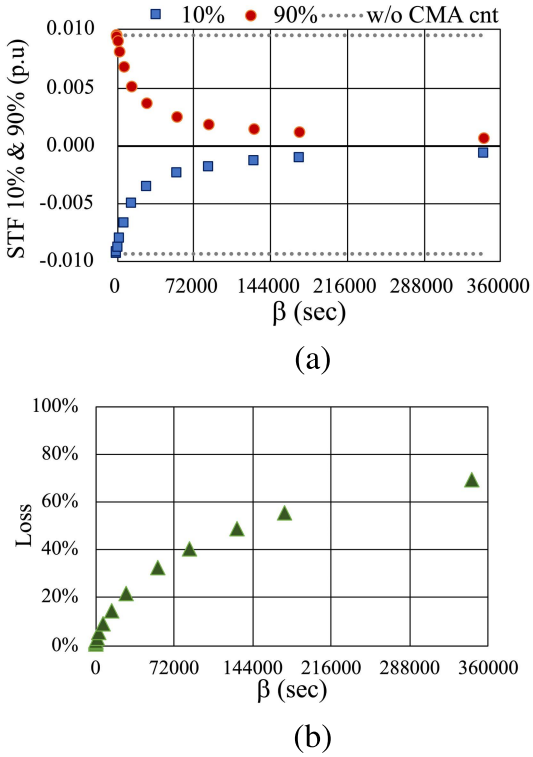

FIGURE 10. Mitigation of STFs by I-RRL in the Tohoku BA. (a) The absolute values of the 10th and 90th percentiles of STFs decreased with β. (b) Energy loss increased with β.

absolute values of the percentiles decreased with α. In the range of $\alpha < 0.02$, the absolute values of the percentiles

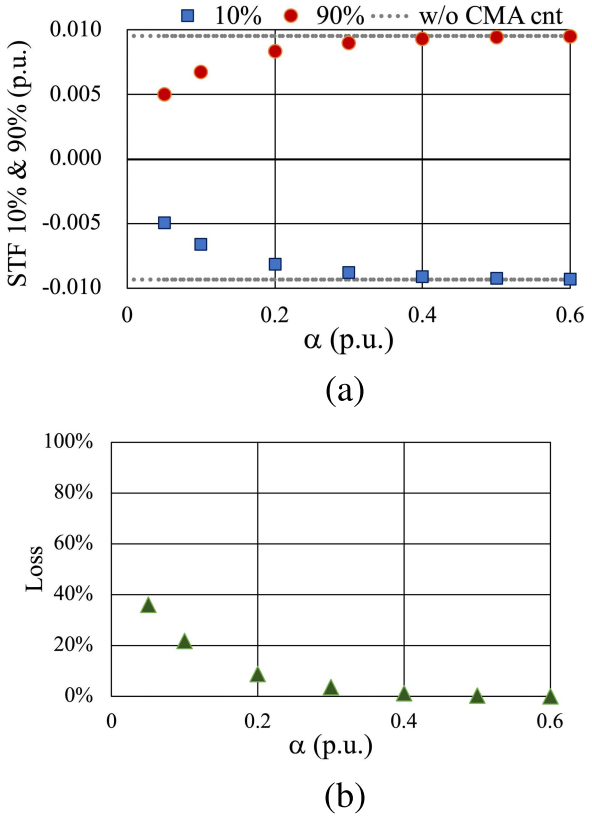

FIGURE 11. Mitigation of STFs by I-MPL in the Tohoku BA. (a) The absolute values of the 10th and 90th percentiles of STFs decreased with α. (b) Energy loss increased as α decreased.

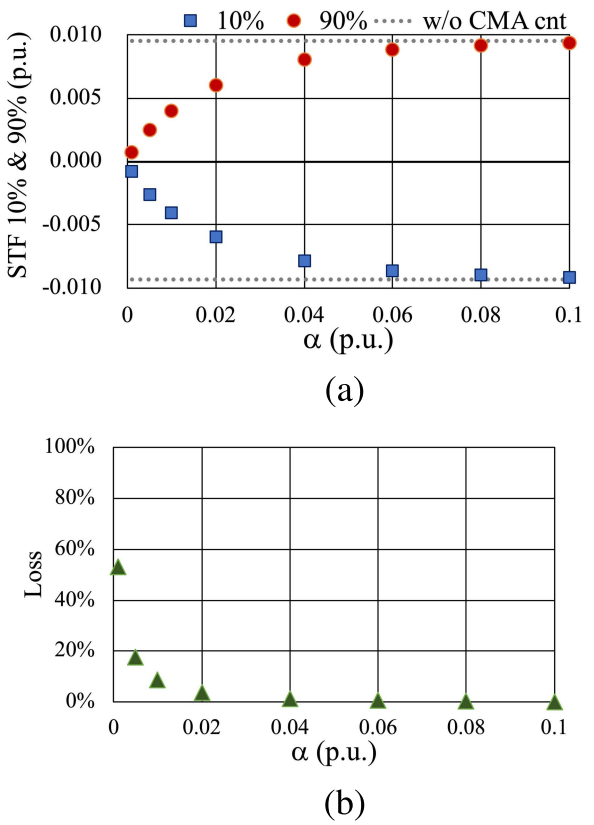

FIGURE 12. Mitigation of STFs by I-AMPL in the Tohoku BA. (a) The absolute values of the 10th and 90th percentiles of STFs decrease with α. (b) The energy loss increases as α decreases.

decreased sharply; the energy loss increased exponentially as α decreased. The relationship between the percentile and energy loss indicates that T-MPL works when α is smaller than 0.02.

Mitigation of STFs by I-RRL in the Tohoku BA is shown in Fig. 10. I-RRL is an available method that uses the same function as the ideal method T-RRL. The degree of mitigation of STFs by I-RRL increased with β. The reduction in amplitude using I-RRL was larger than that of T-RRL, and the energy loss with I-RRL increased to around 70%, as shown in Fig. 10 (b), whereas that with T-RRL was less than 40%, as shown in Fig. 8 (b).

Mitigation of STFs by I-MPL in the Tohoku BA is shown in Fig. 11. I-MPL is an available method that uses the same function as T-MPL. I-MPL calculates the upper limit using output data up to 1 minute before, which differs significantly from I-RRL, which can use up to the immediately preceding output data. The absolute values of the percentiles of I-MPL tended to be larger than those of T-MPL. At $\alpha = 0.05$, the absolute values of the percentiles of I-MPL were about 0.005 (p.u.), and the energy loss was 36%. In the case of T-MPL, as shown in Fig. 9 at $\alpha = 0.005$, while the absolute values of the percentiles were around 0.005 (p.u.) similar to I-MPL, the energy loss was 4%, which is less than a quarter of that of I-MPL. Thus, the efficiency of I-MPL was less than that of T-MPL.

Mitigation of STFs by I-AMPL in the Tohoku BA is shown in Fig. 12. I-AMPL is an available method that uses the same functions as T-MPL and I-MPL. I-AMPL improves the way in which output reduction is shared among individual WPPs. At $\alpha = 0.02$, the absolute values of the percentiles of I-AMPL were about 0.006 (p.u.), and the energy loss was 4%. When the energy losses of T-MPL and I-MPL were about 4%, the absolute values of the percentiles were 0.005 (p.u.) at $\alpha = 0.005$ and 0.008 (p.u.) at $\alpha = 0.3$, respectively. Thus, the efficiency of I-AMPL was higher than that of I-MPL, and approximately the same as that of T-MPL.

To compare the five methods for the three BAs, we examined the relationship between the 10th and 90th percentiles of STFs relative to the total outputs and energy loss, as shown in Fig. 13. The data in Fig. 13 (b) are the same ones in Figs. 8-12. The parameters, α and β, for each method are common among the three BAs. The efficiency of I-AMPL was the highest among the available methods (I-RRL, I-MPL, and I-AMPL), and was equal to the ideal methods (T-RRL and T-MPL) (which exhibited the maximum efficiency). Curves of T-RRL (gray open circles) and T-MPL (red filled triangles) were closer to the x-axis in the figure than those of the other methods, across all of the BAs. Curves close to the x-axis indicate that the absolute values of the percentiles are smaller than for the other methods, with the same amount of energy loss.

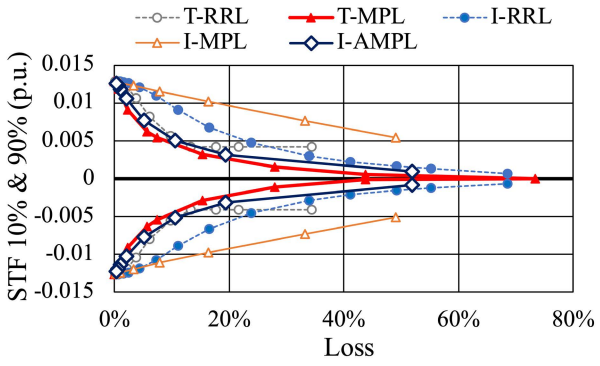

(a) Hokkaido BA

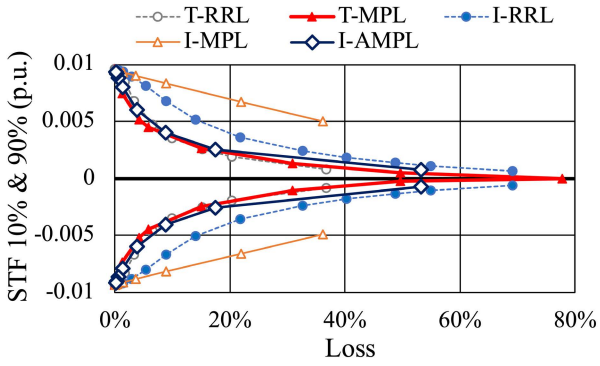

(b) Tohoku BA

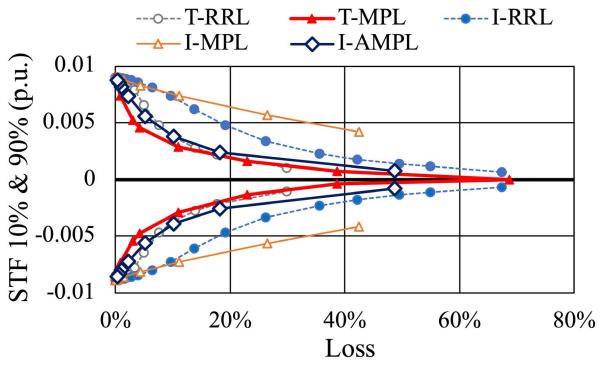

(c) Kyushu BA

FIGURE 13. Relationship between energy loss and the 10th and 90th percentiles of STFs relative to the mitigated total outputs, in the Hokkaido (a), Tohoku (b), and Kyushu (c) BAs.

Despite being one of the three available methods, the efficiency of I-AMPL was similar to T-RRL and T-MPL. When I-AMPL was reduced by half, the energy loss was less than 10%. Note that I-MPL (orange open triangles), which uses the same function as I-AMPL, is the outermost curve and thus has the lowest efficiency. The difference between I-AMPL and I-MPL lies in the way in which the output reduction is shared among the individual WPPs, which is key for improving the efficiency.

From a technical standpoint, the choice of parameter α should be adjusted in the range where the amplitude of the STFs decreases rapidly when α is reduced. However, we note that, when applied to actual WPP groups, it may be set beyond the range if it is worthwhile to mitigate the STF even if energy losses increase. The desired balance between energy loss and mitigation of the STFs in energy system operation also needs to consider the cost-effectiveness of comparing different system operation options for each energy system.

VI. CONCLUSION AND DISCUSSION

Wind power output can fluctuate significantly according to the weather conditions. Rapid growth in the share of wind power generation can make it difficult to operate power systems, due to the major influence of fluctuations in wind power output.

The fluctuations in wind power output can be separated into several categories depending on the time scale. Here, we distinguished VSTFs, STFs, and LTFs using the CMAs; the time scales of the VSTFs and STFs are shorter than 1 minute and 1 hour, respectively; the time scale of the LTFs is longer than those of the VSTFs and STFs.

We focused on STFs in wind power output, and proposed methods to mitigate STFs in the total output of wind power in each BA, based on the RRL and MPPT functions of each wind turbine. The RRL keeps the increment of output below a fixed parameter. The MPPT ensures that the output remains below the upper limit, according to the control signal sent from an aggregator. We assumed that the WFC in each WPP appropriately controlled each wind turbine in the WPP.

To evaluate the proposed methods, numerical simulations were performed using historical wind power output data from three Japanese BAs: the Hokkaido, Tohoku, and Kyushu BAs. The proposed methods were categorized into ideal and available methods. The ideal methods use the total output of wind power in each BA. The available methods use the wind power outputs from individual WPPs. The ideal methods cannot be applied in the real world because the total output data are obtained based on the individual outputs of all WPPs. STF mitigation using the ideal methods represents a best-case scenario, as the total output benefits from the smoothing effect; thus, the ideal methods were used as a reference for comparison with the available methods.

The relationship between STF mitigation and energy loss indicates the efficiency of the method. Thus, even if the mitigation of STFs is considerable, efficiency is low when the energy loss is extremely large. We found that the efficiency of one of the available methods was nearly the same as that of the two ideal methods. Additionally, despite using the MPPT, the method in question achieved the highest efficiency, although its counterpart using the same MPPT showed the worst efficiency. The difference between the best and worst available methods lies in the way in which the reduction in output is shared among the WPPs in the BA. The best available method shares the output reduction depending on the previous outputs from each WPP. Thus, the upper limits of the individual outputs differ depending on the previous output of the WPP.

The method of sharing the output reduction among WPPs is a key factor for improving efficiency.

In addition, the results were similar among the three BAs. We believe that the best method could be applied successfully to other BAs; however, additional research is necessary to identify the optimal method. Wind power capacity has been increasing all over the world, and the share of the wind power also increases. Therefore, when the latest wind power output data are available, applying the methods to the data is required.

We used the 10th and 90th percentiles of STFs to evaluate the mitigation methods. The methods intend to overcome difficulties of system operations under conditions of rapid wind power growth. We consider that there may be more appropriate indicators to evaluate the method from the perspective of system operations. While the indicator is an important issue, a work to find more appropriate indicators is beyond the scope of this paper and will be our future work.

Methods to mitigate STFs in wind power output are an essential step on the road toward RE100. To further improve the methods, several approaches are available, such as utilization of wind power forecasting and machine learning technologies. When wind power forecasting has high accuracy, the energy loss can be reduced. Note that suitable short-term forecasting to apply the mitigation methods should be chosen. Machine learning technologies could provide more appropriate parameter settings and control signals for individual WPPs to effectively mitigate STFs. There are a number of combinations between types of machine learning methods and ways to apply them to the mitigation methods. It is crucial to narrow down the candidates of the combinations. Therefore, utilization of machine learning technologies will also be our future work.

The RRL and MPPT are available not only for wind power, but also for solar power. Therefore, the proposed methods could be adopted to mitigate STFs in solar power output. In addition, when the price of energy storage decreases sufficiently, wind and solar power outputs can be charged into storage, instead of reducing the output. It is expected that the proposed methods will be adopted to provide signals to charge into storage, thus allowing power system operations to attain RE100.

APPENDICES A DATA CORRECTION AND MISSING DATA

There were missing raw wind power output data [6]. Missing data were linearly interpolated when the period of the missing data was less than 3 hours. When the period of missing data was at least 3 hours, the data were removed from the time series. While the Tohoku and Kyushu BAs did not have missing data with a period of more than 3 hours, the percentage of such missing data with respect to the entire dataset was 12.5% in the Hokkaido BA. The missing data in the Hokkaido BA are attributable to signal transfer errors from WPPs to the data aggregation system.

REFERENCES

[1] International Renewable Energy Agency. (2020). *Renewable Energy Statistics 2020*. [Online]. Available: https://www.irena.org/publications/2020/Jul/Renewable-energy-statistics-2020

[2] International Renewable Energy Agency. (2021). *Renewable Energy Statistics 2021*. [Online]. Available: https://irena.org/publications/2021/Aug/Renewable-energy-statistics-2021

[3] J. Widén, N. Carpman, V. Castellucci, D. Lingfors, J. Olauson, F. Remouit, M. Bergkvist, M. Grabbe, and R. Waters, "Variability assessment and forecasting of renewables: A review for solar, wind, wave and tidal resources," *Renew. Sustain. Energy Rev.*, vol. 44, pp. 356–375, Apr. 2015.

[4] D. Liu, J. Guo, Y. Huang, and W. Wang, "An active power control strategy for wind farm based on predictions of wind turbine's maximum generation capacity," *J. Renew. Sustain. Energy*, vol. 5, no. 1, Jan. 2013, Art. no. 013121.

[5] H. Holttinen, "Impact of hourly wind power variations on the system operation in the Nordic countries," *Wind Energy*, vol. 8, no. 2, pp. 197–218, 2005.

[6] C. T. Urabe, T. Saitou, K. Kataoka, T. Ikegami, and K. Ogimoto, "Positive correlations between short-term and average long-term fluctuations in wind power output," *Energies*, vol. 14, no. 7, p. 1861, Mar. 2021.

[7] International Energy Agency. (2014). *The Power of Transformation*. [Online]. Available: https://iea.blob.core.windows.net/assets/b6a02e69-35c6-4367-b342-2acf14fc9b77/The_power_of_Transformation.pdf

[8] M. Huber, D. Dimkova, and T. Hamacher, "Integration of wind and solar power in Europe: Assessment of flexibility requirements," *Energy*, vol. 69, pp. 236–246, May 2014.

[9] International Energy Agency. (2016). *Re-Powering Markets*. [Online]. Available: https://iea.blob.core.windows.net/assets/4452f4ea-59d0-497b-8736-069b4cb39851/REPOWERINGMARKETS.pdf

[10] Z. Wu, M. Zhou, G. Li, T. Zhao, Y. Zhang, and X. Liu, "Interaction between balancing market design and market behaviour of wind power producers in China," *Renew. Sustain. Energy Rev.*, vol. 132, Oct. 2020, Art. no. 110060.

[11] European Network of Transmission System Operators for Electricity. (2018). *Electricity Balancing in Europe*. [Online]. Available: https://www.entsoe.eu/news/2018/12/12/electricity-balancing-in-europe-entso-e-releases-an-overview-of-the-european-electricity-balancing-market-and-guideline

[12] *Transmission and Distribution Network Operation Committee, 13th Balancing Market Subcommittee*, document 3, 2019. [Online]. Available: https://www.occto.or.jp/iinkai/chouseiryoku/jukyuchousei/2019/2019_jukyuchousei_13_haifu.htmlinJapanese

[13] JapanWind Power Association. (2021). *Wind Power Cumulative Capacity in Japan at the End of 2021*. [Online]. Available: https://jwpa.jp/information/6225/inJapanese

[14] Agency for Natural Resources and Energy, Ministry of Economy, Trade and Industry. (2021). *Electric Power Survey Statistics*. [Online]. Available: https://www.enecho.meti.go.jp/statistics/electric_power/ep002/index.htmlinJapanese

[15] I. D. Margaris, S. A. Papathanassiou, N. D. Hatziargyriou, A. D. Hansen, and P. Sorensen, "Frequency control in autonomous power systems with high wind power penetration," *IEEE Trans. Sustain. Energy*, vol. 3, no. 2, pp. 189–199, Apr. 2012.

[16] S.-E. Lee, D.-J. Won, and I.-Y. Chung, "Operation scheme for a wind farm to mitigate output power variation," *J. Electr. Eng. Technol.*, vol. 7, no. 6, pp. 869–875, Nov. 2012.

[17] J. Lin, Y. Sun, Y. Song, W. Gao, and P. Soensen, "Wind power fluctuation smoothing controller based on risk assessment of grid frequency deviation in an isolated system," *IEEE Trans. Sustain. Energy*, vol. 4, no. 2, pp. 379–392, Apr. 2013.

[18] H. Meng, T. Yang, J.-Z. Liu, and Z. Lin, "A flexible maximum power point tracking control strategy considering both conversion efficiency and power fluctuation for large-inertia wind turbines," *Energies*, vol. 10, no. 7, p. 939, Jul. 2017.

[19] M. Dreidy, H. Mokhlis, and S. Mekhilef, "Inertia response and frequency control techniques for renewable energy sources: A review," *Renew. Sustain. Energy Rev.*, vol. 69, pp. 144–155, Mar. 2017.

[20] A. Aziz, A. T. Oo, and A. Stojcevski, "Frequency regulation capabilities in wind power plant," *Sustain. Energy Technol. Assessments*, vol. 26, pp. 47–76, Apr. 2018.

[21] V.-H. Bui, A. Hussain, and H.-M. Kim, "Optimal operation of wind farm for reducing power deviation considering grid-code constraints and events," *IEEE Access*, vol. 7, pp. 139058–139068, 2019.

[22] X. Zhao-xia, Z. Mingke, H. Yu, J. M. Guerrero, and J. C. Vasquez, "Coordinated primary and secondary frequency support between microgrid and weak grid," *IEEE Trans. Sustain. Energy*, vol. 10, no. 4, pp. 1718–1730, Oct. 2019.
[23] S. I. Abouzeid, Y. Guo, and H.-C. Zhang, "Dynamic control strategy for the participation of variable speed wind turbine generators in primary frequency regulation," *J. Renew. Sustain. Energy*, vol. 11, no. 1, Jan. 2019, Art. no. 013304.
[24] *Wind Energy Generation Systems—Part 1: Design Requirements*, Standard IEC 61400-1:2019, International Electrotechnical Commission, 2019. [Online]. Available: https://webstore.iec.ch/publication/26423
[25] *Wind Energy Generation Systems—Part 3–1: Design Requirements for Fixed Offshore Wind Turbines*, Standard IEC 61400-3-1:2019, 2019. [Online]. Available: https://webstore.iec.ch/publication/29360
[26] *Wind Energy Generation Systems—Part 3–2: Design Requirements for Floating Offshore Wind Turbines*, Standard IEC TS 61400-3-2:2019, 2019. [Online]. Available: https://webstore.iec.ch/publication/29244
[27] S. Martin-Martinez, E. Gómez-Lazaro, A. Vigueras-Rodríguez, J. A. Fuentes-Moreno, and A. Molina-Garcia, "Analysis of positive ramp limitation control strategies for reducing wind power fluctuations," *IET Renew. Power Gener.*, vol. 7, no. 6, pp. 593–602, 2013.
[28] F. Díaz-González, M. Hau, A. Sumper, and O. Gomis-Bellmunt, "Participation of wind power plants in system frequency control: Review of grid code requirements and control methods," *Renew. Sustain. Energy Rev.*, vol. 34, pp. 551–564, Jun. 2014.
[29] H. Badihi, Y. Zhang, and H. Hong, "Active power control design for supporting grid frequency regulation in wind farms," *Annu. Rev. Control*, vol. 40, pp. 70–81, Jan. 2015.
[30] V. Gevorgian, Y. Zhang, and E. Ela, "Investigating the impacts of wind generation participation in interconnection frequency response," *IEEE Trans. Sustain. Energy*, vol. 6, no. 3, pp. 1004–1012, Jul. 2015.
[31] R. M. Kamel, "Standalone micro grid power quality improvement using inertia and power reserves of the wind generation systems," *Renew. Energy*, vol. 97, pp. 572–584, Nov. 2016.
[32] X. X. Zhao, Z. H. Yan, Y. Xue, and X. P. Zhang, "Wind power smoothing by controlling the inertial energy of turbines with optimized energy yield," *IEEE Access*, vol. 5, pp. 23374–23382, 2017.
[33] M. Ramírez-González, R. Castellanos-Bustamante, J. G. Calderón-Guizar, and O. P. Malik, "Assessment of inertial and primary frequency control from wind power plants in the Mexican electric power grid," *WIREs Energy Environ.*, vol. 8, no. 6, p. e356, Nov. 2019.
[34] L. Ye, C. Zhang, Y. Tang, W. Zhong, Y. Zhao, P. Lu, B. Zhai, H. Lan, and Z. Li, "Hierarchical model predictive control strategy based on dynamic active power dispatch for wind power cluster integration," *IEEE Trans. Power Syst.*, vol. 34, no. 6, pp. 4617–4629, Nov. 2019.
[35] P. Mahish and A. K. Pradhan, "Distributed synchronized control in grid integrated wind farms to improve primary frequency regulation," *IEEE Trans. Power Syst.*, vol. 35, no. 1, pp. 362–373, Jan. 2020.
[36] J. I. Yoo, Y. C. Kang, D. Yang, K.-H. Kim, and J.-W. Park, "Power smoothing of a variable-speed wind turbine generator based on a two-valued control gain," *IEEE Trans. Sustain. Energy*, vol. 11, no. 4, pp. 2765–2774, Oct. 2020.
[37] S. Siniscalchi-Minna, F. D. Bianchi, C. Ocampo-Martinez, J. L. Domínguez-García, and B. De Schutter, "A non-centralized predictive control strategy for wind farm active power control: A wake-based partitioning approach," *Renew. Energy*, vol. 150, pp. 656–669, May 2020.
[38] X. Lyu, Y. Jia, and Z. Xu, "A novel control strategy for wind farm active power regulation considering wake interaction," *IEEE Trans. Sustain. Energy*, vol. 11, no. 2, pp. 618–628, Apr. 2020.
[39] G. Ferro, M. Robba, and R. Sacile, "A model predictive control strategy for distribution grids: Voltage and frequency regulation for islanded mode operation," *Energies*, vol. 13, no. 10, p. 2637, May 2020.
[40] T. Ikegami, C. T. Urabe, T. Saitou, and K. Ogimoto, "Numerical definitions of wind power output fluctuations for power system operations," *Renew. Energy*, vol. 115, pp. 6–15, Aug. 2018.
[41] G. Sinden, "Characteristics of the U.K. wind resource: Long-term patterns and relationship to electricity demand," *Energy Policy*, vol. 35, no. 1, pp. 112–127, Jan. 2007.
[42] B. Hasche, "General statistics of geographically dispersed wind power," *Wind Energy*, vol. 13, no. 8, pp. 773–784, Nov. 2010.
[43] J. Widen, "Correlations between large-scale solar and wind power in a future scenario for Sweden," *IEEE Trans. Sustain. Energy*, vol. 2, no. 2, pp. 177–184, Apr. 2011.
[44] J. Olauson and M. Bergkvist, "Correlation between wind power generation in the European countries," *Energy*, vol. 114, pp. 663–670, Nov. 2016.
[45] T. Enomoto, T. Ikegami, C. T. Urabe, T. Saitou, and K. K. Ogimoto, "Geographical smoothing effects on wind power output variation in Japan," *Int. J. Smart Grid Clean Energy*, vol. 7, no. 3, pp. 188–194, 2018.

CHIYORI T. URABE (Member, IEEE) received the bachelor's and Master of Physics degrees in nonlinear physics from Nara Women's University, Japan, in 1998 and 2000, respectively, and the Doctor of Philosophy degree in nonequilibrium statistical physics from Kyoto University, Japan, in 2006. She is currently working as a Project Assistant Professor with the Institute of Industrial Science, The University of Tokyo, Japan. Her research interests include renewable energy and energy system integration.

TAKASHI IKEGAMI (Member, IEEE) received the B.E. and M.E. degrees in chemical system engineering and the Ph.D. degree in urban engineering from The University of Tokyo, in 2001, 2003, and 2007, respectively. He then worked as a Postdoctoral Researcher at the National Institute for Environmental Studies, and he later worked as a Project Assistant Professor at the University of Tokyo. Since 2014, he has been an Associate Professor at the Tokyo University of Agriculture and Technology. His current research interests include the system analysis using the mathematical programming for energy system equipment planning and operation, concerned with renewable energy sources and demand response for power system operation. He is a member of the Japan Society of Civil Engineers (JSCE) and the Japan Society of Energy and Resources (JSER).

KAZUHIKO OGIMOTO (Member, IEEE) graduated from The University of Tokyo. He joined a wholesale power company, JPOWER. With JPOWER, he worked for power system planning, research and development of a SMES, renewable energy, a voltage source converter, a hydrogen energy system, IT application and modernization of plant maintenance, and energy technology development strategy, until 2007. In 2008, he joined The University of Tokyo. His major research interests include energy system integration, energy system management, long-range energy technology strategy, decentralized energy management, and plant maintenance and risk management. Since 2018, he has been leading a member of the Energy System Integration Social Cooperation Program of the Institute.